PHOTONICS Research

Tailoring magnetic dipole emission by coupling to magnetic plasmonic anapole states

Gui-Ming Pan,[1,5] Li-Feng Yang,[2] Fang-Zhou Shu,[3] Yan-Long Meng,[1] Zhi Hong,[3] and Zhong-Jian Yang[4,6]

[1]College of Optical and Electronic Technology, China Jiliang University, Hangzhou 310018, China
[2]First People's Hospital of Changzhou, Changzhou 213000, China
[3]Centre for THz Research, China Jiliang University, Hangzhou 310018, China
[4]Hunan Key Laboratory of Nanophotonics and Devices, School of Physics and Electronics, Central South University, Changsha 410083, China
[5]e-mail: gmpan@cjlu.edu.cn
[6]e-mail: zjyang@csu.edu.cn

Received 19 April 2022; revised 19 May 2022; accepted 9 June 2022; posted 10 June 2022 (Doc. ID 461415); published 15 August 2022

The interaction between magnetic quantum emitters and the local electromagnetic environment is a promising method to manipulate the spontaneous emission. However, it is severely limited by the weak interactions between the magnetic component of light and natural materials. Herein, we demonstrate that the special type of anapole states associated with the "onefold" electric toroidal dipole moment can be excited by efficient interaction between magnetic dipole emitters and silver oligomers. Based on magnetic anapole states, the radiative power is effectively suppressed with significant coupling between the emitter and the silver nonamer, physically providing an ideal playground for the study of non-radiative transitions. These findings not only introduce magnetic anapoles to plasmonics but also open a door for the development of new high-performance magnetic-dipole-based optoelectronic devices.

https://doi.org/10.1364/PRJ.461415

1. INTRODUCTION

Magnetic dipole (MD) spontaneous emission is very significant to some transition metals such as Cr^{3+} and lanthanide series ions such as Eu^{3+}, Er^{3+}, Ho^{3+}, and Nd^{3+} that electric dipole (ED) transitions are forbidden to the first order [1–3]. Beyond the characteristics of the common spontaneous emission, MD spontaneous emission has a lot of unique optical properties that have a variety of applications, such as detecting the magnetic component of light [2]. Thus, the effective control of MD spontaneous emission behaviors is very significant to designing new optoelectronic devices, which has attracted tremendous attention in recent years [4–7]. However, MD transitions are inherently weaker than ED transitions. Besides, due to the absence of the magnetic monopole, the interactions between natural materials and the magnetic component of light are also very weak, which seriously limits the external manipulation of MD spontaneous emission behaviors according to the Purcell effect [8–10].

Generally, both the enhancement and suppression of MD radiative power play significant roles in tailoring spontaneous emission. Taking account of the weak transitions of the MD, the enhancement and suppression of the radiative processes should be based on the great enhancement of the transition rates. In the past decade, most of the studies focused on enhancing MD spontaneous emission, but few studies touched the topic of suppressing it [4,11,12]. It was demonstrated that MD spontaneous emission can be effectively enhanced in artificial nanostructures supporting MD resonances [4,11,12]. Recently, a small number of studies considered the suppression of MD spontaneous emission [2,13]. Based on the destructive interaction between the MD moment of emitter itself and the induced MD moment of the nanostructures, the radiative power of MD emitters can be efficiently suppressed [4,13]. But this method is applicable only in a weak coupling context where the MD moment of the emitter itself and the induced MD moment are in the same magnitude. The MD transitions are not enhanced when the radiative power is suppressed. Physically, the destructively coherent modes generated by the efficient coupling between the MD emitters and the nanostructures are crucial to suppress the radiative power.

Very recently, anapole states associated with the great enhancement of near-field and suppression of corresponding multipole scattering have had great implications for manipulating spontaneous emission behaviors [14–19]. Anapole states are excited by the destructive interferences between Cartesian electromagnetic multipole moments and Cartesian toroidal moments that can be divided into electric and magnetic types [20–23]. However, most previous studies show that the Cartesian electric toroidal dipole (ETD) moments correlated with the circulating

magnetic field are excited by two or more electric current loops. More than one electric current loops exhibit high-order magnetic resonances [14,24–26]. In a high symmetric system, the optical modes with different angular momentum cannot effectively interact with each other [27–29]. Thus, the significant coupling between the MD point sources and high-symmetry nanostructures is expected to generate strong MD moments instead of ETD moments. Therefore, the challenge of manipulating MD spontaneous emission via anapole states is that the mode-matching condition cannot be met.

Nevertheless, surface plasmon resonance (SPR) may bring the opportunities to solve this problem. Based on the plasmon hybridization, the noble metal oligomers that can be considered as plasmonic metamolecules are the good platforms for studying the magnetic component of light [30–33]. The electric, magnetic, and toroidal multipoles can be easily excited by a plane wave or a point source by properly designing the spatial distributions of the plasmonic metamolecules [34–36]. In addition, SPR can reduce the mode volumes and increase the local state densities by concentrating light in subwavelength scale, leading to the improvement of transition rates [37,38].

In this paper, we demonstrate that the MD spontaneous emission can be effectively manipulated by the plasmonic anapole states associated with the "onefold" toroidal moments in silver oligomers. The so-called "onefold" Cartesian ETD moment is related to the circulating magnetic field that is excited by an asymmetric electric current loop. Meanwhile, this electric current loop correlating with MD resonance indicates that the onefold ETD will be excited by efficient coupling between the MD emitters and plasmonic metamolecules. Besides, the head-to-tail onefold Cartesian ETDs form a circulating electric component of light that leads to the excitation of the Cartesian magnetic toroidal dipole (MTD) moment in a silver nonamer. The magnetic anapole state is generated by the destructive interference between the Cartesian MTD moment and the Cartesian MD moment induced by the MD emitters [39]. Based on the magnetic anapole state, the MD radiative power is remarkably suppressed with the significant coupling between the emitter and the silver nonamer, which acts rather like the non-radiative transitions [40]. This study not only introduces magnetic anapoles to plasmonics but also provides new thinking for developing high-performance magnetic-dipole-based optoelectronic devices.

2. ELECTRIC ANAPOLE STATES BASED ON ONEFOLD ETD MOMENTS

According to classical electrodynamics, the electric field and magnetic field can excite each other, which defers to Ampére's rule [41,42]. The symmetric circulating electric field is expected to excite the vertical magnetic field [41]. However, when the symmetry is broken, the vertical magnetic field will bend, forming an MD moment and a circulating magnetic field, shown in Fig. 1(a). The onefold Cartesian ETD moment is generated by the circulating magnetic field. Besides, the asymmetric circulating electric current also gives rise to an ED moment. Then, the electric anapole condition is achieved via the destructive interference between the Cartesian ED and ETD moment. Moreover, the head-to-tail Cartesian ETD moments can form a circulating electric

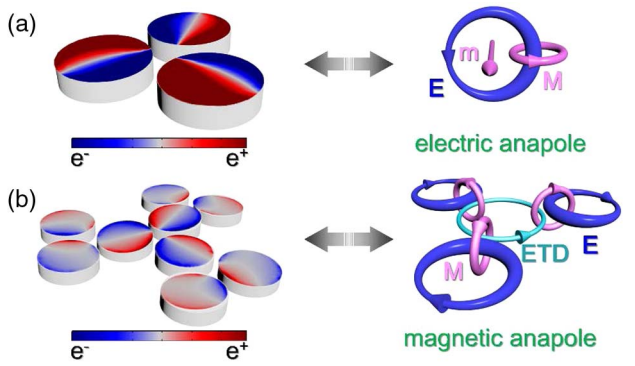

Fig. 1. Illustration of the excitation of the (a) electric and (b) magnetic anapole states. The surface charge distributions of the silver trimer and nonamer at the wavelength of the electric and magnetic anapole states suggest the multipole configurations. The dark green ring shows the head-to-tail Cartesian ETD moments.

component of light, leading to the generation of the Cartesian MTD moment, as shown in Fig. 1(b). The magnetic anapole state is excited by the out-of-phase coupling between the Cartesian MD moment and the Cartesian MTD moment, leading to the suppression of the spherical MD scattering.

In order to verify it, a silver trimer consisting of three nanodisks is designed. It should be noted that this structure supports MD resonance and has been reported both analytically and experimentally in many previous works [43–45]. A monochromatic plane wave propagates along the z axis with the angle $\theta = 80°$ and is polarized along the x axis, shown in Fig. 2(a). The silver trimer is suspended in the air with refractive index $n = 1$. The refractive index data describing the optical response of silver is given by Johnson and Christy [46]. The multipole decomposition of the light scattering cross sections and scattering power are calculated using the finite element method performed by the commercial COMSOL Multiphysics software. We consider that all of the electric and magnetic multipoles locate at the center of mass of the silver trimer. The electric and magnetic multipole coefficients in spherical coordinates are given as [47]

$$a(l,m) = \frac{(-i)^{l-1}k^2 Z_0 O_{lm}}{E_0[\pi(2l+1)]^{1/2}} \cdot \int e^{-im\phi} \cdot \left\{ [\psi_l(kr) + \psi''_l(kr)] P_l^m(\cos\theta)\hat{r}\cdot \boldsymbol{J}_{\mathrm{sca}}(\boldsymbol{r}) + \frac{\psi'_l(kr)}{kr} \cdot \left[\frac{\mathrm{d}}{\mathrm{d}\theta} P_l^m(\cos\theta)\hat{r}\cdot \boldsymbol{J}_{\mathrm{sca}}(\boldsymbol{r}) - i\frac{m}{\sin\theta} P_l^m(\cos\theta)\hat{\phi}\cdot \boldsymbol{J}_{\mathrm{sca}}(\boldsymbol{r}) \right] \right\} \mathrm{d}^3 r, \quad (1)$$

$$b(l,m) = \frac{(-i)^{l+1}k^2 Z_0 O_{lm}}{E_0[\pi(2l+1)]^{1/2}} \cdot \int e^{-im\phi} j_l(kr) \left[i\frac{m}{\sin\theta} P_l^m(\cos\theta)\hat{\theta}\cdot \boldsymbol{J}_{\mathrm{sca}}(\boldsymbol{r}) + \frac{\mathrm{d}}{\mathrm{d}\theta} P_l^m(\cos\theta)\hat{\phi}\cdot \boldsymbol{J}_{\mathrm{sca}}(\boldsymbol{r}) \right] \mathrm{d}^3 r, \quad (2)$$

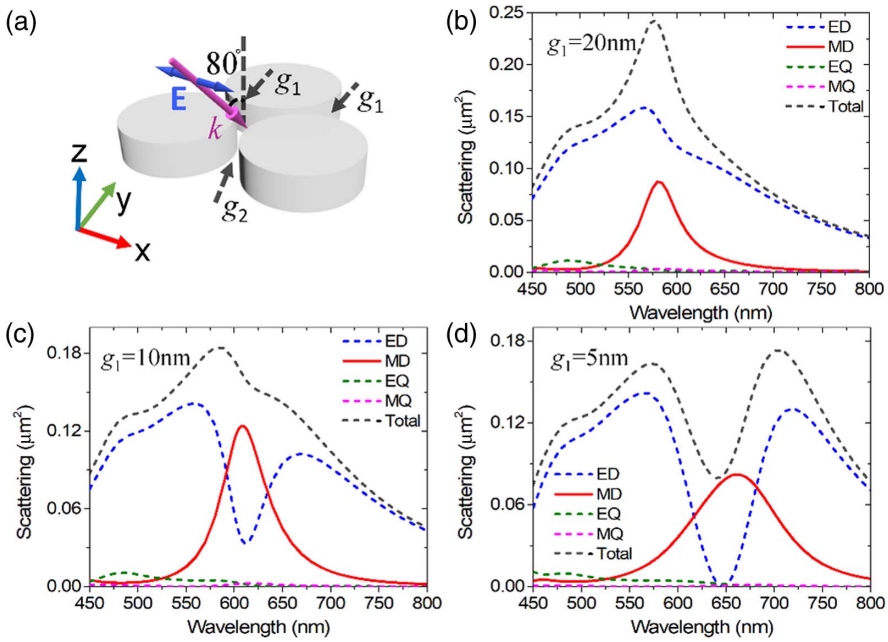

Fig. 2. Scattering cross sections and their spherical multipole decomposition calculated for the silver trimers. (a) Schematic of the silver trimer that consists of three same-sized nanodisks with the radii $r = 61$ nm. The thickness of three silver disks is 40 nm, and the incident angle $\theta = 80°$. (b) Evenly spaced three silver nanodisks with the gaps $g_1 = g_2 = 20$ nm; (c) $g_1 = 10$ nm, $g_2 = 20$ nm; (d) $g_1 = 5$ nm, $g_2 = 20$ nm.

where l and m denote the order of the multipole components and the amount of the z component of angular momentum, respectively. $\boldsymbol{J}_{\text{sca}}(\boldsymbol{r}) = -i\omega[\varepsilon(\boldsymbol{r}) - \varepsilon_h]\boldsymbol{E}(\boldsymbol{r})$ (ε_h is the dielectric constant of the surrounding medium) and Z_0 are the scattering current density and impedance, respectively. O_{lm} reads $O_{lm} = [(2l+1)(l-m)!/(l+m)!]^{1/2}[4\pi l(l+1)]^{-1/2}$. $\psi_l(kr)$ given by the Riccati–Bessel function. $P_m^l(\cos\theta)$ represents the associated Legendre polynomials. E_0 is the electric field amplitude of the incident light. θ and φ are the zenith angle and azimuthal angle, respectively.

The lth order electric and magnetic multipole scattering cross sections are expressed as

$$\sigma_E^l = \frac{\pi}{k^2}\sum_{m=-l}^{l}(2l+1)|a(l,m)|^2, \tag{3}$$

$$\sigma_M^l = \frac{\pi}{k^2}\sum_{m=-l}^{l}(2l+1)|b(l,m)|^2. \tag{4}$$

The multipole cross sections of the silver trimers are shown in Fig. 2. According to Fig. 2(b), there is a broad ED scattering peak at the wavelength of 582 nm with the weak MD overlapping spectrum in the symmetric silver trimer. If reducing the gaps g_1, the ED spectrum exhibits a dip at the wavelength of 612 nm, shown in Fig. 2(c). On the contrary, the contribution of the MD component increases. Continuing to reduce g_1, the ED component can be further suppressed at the wavelength of 647 nm, and the proportion of the MD component increases, shown in Fig. 2(d). The previous reports claimed that the dip is magnetic-based Fano resonance excited by the ED mode and MD mode [43,44]. In fact, the suppression of the ED is based on the achievement of the anapole state. As the coherent modes, both the Cartesian ED moment and ETD moment are "bright modes" that can be directly excited by the incident wave. The totally destructive interference between the Cartesian ED moment and ETD moment is allowed, leading to the complete suppression of the ED moment [14].

To validate the analyses above, the Cartesian ED and ETD cross sections are calculated [48],

$$\sigma_{\text{sca}}^{\text{ED}} = \frac{c^2k^4Z}{12\pi I_0}|\boldsymbol{p}|^2, \tag{5}$$

$$\sigma_{\text{sca}}^{\text{ETD}} = \frac{c^2k^6Z}{12\pi I_0}|\boldsymbol{T}(e)|^2, \tag{6}$$

where $\boldsymbol{p} = -\int \mathrm{d}r^3\boldsymbol{J}_{\text{sca}}(\boldsymbol{r})/i\omega$ is the Cartesian ED moment and $\boldsymbol{T}(e) = \int \mathrm{d}r^3\{[\boldsymbol{r}\cdot\boldsymbol{J}_{\text{sca}}(\boldsymbol{r})]\boldsymbol{r} - 2r^2\boldsymbol{J}_{\text{sca}}(\boldsymbol{r})\}/10c$ is the Cartesian ETD moment. $\boldsymbol{J}_{\text{sca}}(\boldsymbol{r})$ is the scattering current density, and I_0 is illumination intensity of the incident plane wave. The ideal anapole condition is achieved, where $\boldsymbol{p} = -ik\boldsymbol{T}(e)$ is satisfied [14].

Though the Cartesian ETD moment can be excited by the asymmetric circulating electric current shown in Fig. 3(a), the relative strong electric field between the gap of the two bottom nanodisks forms the strong ED moment in the equidistant silver trimer. Thus, the spherical ED scattering is expected to exhibit Lorentzian line shape. But according to the phase of the Cartesian ED and ETD moments shown in Fig. 3(a), the out-of-phase coupling leads to the suppression of the spherical ED moment to some extent. Thus, the spherical ED scattering exhibits a small dip at the wavelength of 582 nm. Reducing the gaps g_1 will increase the overlap between the top and the two bottom nanodisks, leading to the increase

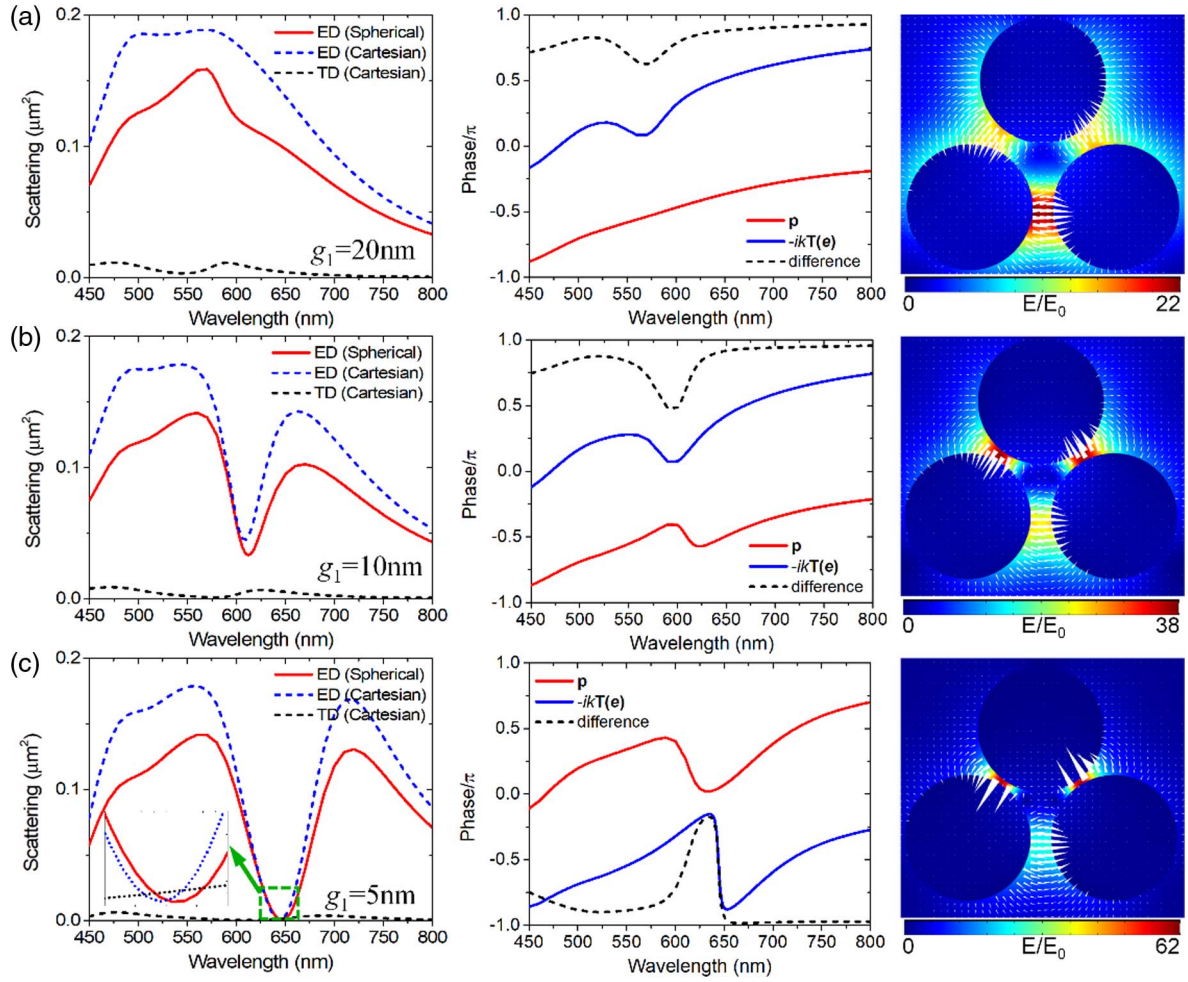

Fig. 3. Spherical ED, Cartesian ED, Cartesian ETD scattering cross sections, and the phase of Cartesian TD and Cartesian ETD moments with the corresponding electric near-field distributions of the silver trimers at the dips of spherical ED spectra. (a) $g_1 = 20$ nm, (b) $g_1 = 10$ nm, (c) $g_1 = 5$ nm, respectively. The white arrows indicate the directions of the *E*-field.

of the coupling strength between these nanodisks. The relative strong electric near-field between the top and the two bottom nanodisks excites the circulating magnetic field that leads to the generation of the remarkable Cartesian ETD moment, shown in Fig. 3(b). The phase difference between the Cartesian ETD and Cartesian ED moments is about π, which indicates the destructive interference between them. Then the anapole state is excited at the wavelength of 612 nm. Continuing to reduce g_1 will further increase the coupling strength between the modes supported by the top and the two bottom nanodisks. Then, the stronger coupling between the Cartesian ED and ETD moments leads to the total suppression of spherical ED scattering, and the ideal anapole state is achieved at the wavelength of 647 nm, shown in Fig. 3(c). It should be noted that reducing incident angle θ will decrease the overlap between the top and the two bottom nanodisks, leading to the weak coupling between the Cartesian ED and ETD moments. The theoretical results are compatible with the experimental results [43]. The excitation of the electric anapole state suggests that the Cartesian ETD moment can be effectively generated by an asymmetric electric current loop. In addition, due to the circulating magnetic field excited by one asymmetric electric field loop, we expect a stronger MD scattering cross section peak at the wavelength of the anapole condition. If the circulating magnetic field is excited by two or more electric loops, the corresponding high-order magnetic cross section peak will be weaker than that in this work.

3. TAILORING MD EMISSION BEHAVIOR BY THE MAGNETIC ANAPOLE STATE

As a point source, the MD emitter can interact with the plasmonic metamolecules. The optical modes with different angular momenta can be excited via reducing the symmetry of the nanosystems [27]. On one hand, the optical properties of these modes are the spontaneous emission behavior of the MD emitter. On the other hand, the induced local fields of these optical modes will build the electromagnetic environment and have a great influence on the MD transitions of the emitters [8]. In order to tailor MD spontaneous emission to a greater extent, the two processes should be based on the efficient interactions between the MD emitter and the nanostructures. Therefore, the nanostructures should support MD resonance or the modes that can couple with MD modes. To characterize the optical

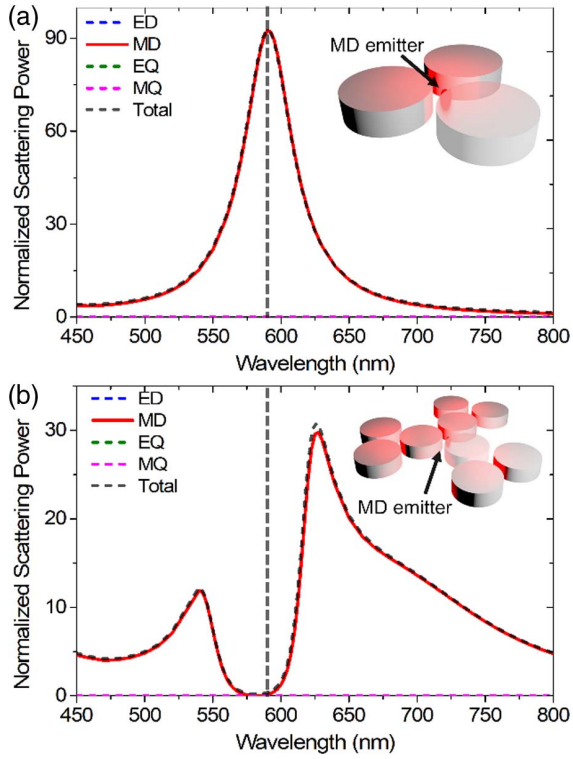

Fig. 4. Normalized multipole scattering power of (a) the silver trimer and (b) the nonamer. The insets are the structure schematics; for the trimer, the radii of the three silver nanodisks are 61 nm with the gap of 16 nm between adjacent ones. The silver nonamer is formed by adding two small nanodisks around every disk of the trimer with the radii of 56 nm and the gap of 10 nm between adjacent ones. The gaps between the small nanodisks and the closest nanodisks of the trimer are 8 nm. The MD emitters are set in the center of the trimer and nonamer with the orientation along the z axis, respectively.

properties of the surroundings, we only take the scattering power emission from the nanostructures into consideration and ignore the power radiated from the emitter itself in the multipole decomposition. In addition, the spherical multipole scattering power decomposition is calculated by revising the coefficients in front of the integral sign as $(-i)^{l-1}k^2O_{lm}/[\pi(2l+1)]^{1/2}$ and $(-i)^{l+1}k_2O_{lm}/[\pi(2l+1)]^{1/2}$ in Eqs. (1) and (2), respectively [6].

According to Fig. 2, the strong MD resonance can be excited in a silver trimer. The MD emitter is set in the center of the silver trimer, and the orientation of the MD moment is perpendicular to the trimer plane. The coupling strength between the MD emitter and the silver trimer is very strong, and the induced MD moment is larger than the dipole moment itself, with nearly all power emitted from the silver trimer scattering. Thus, the normalized MD scattering power exhibits a Lorentzian line shape, and the contributions of other multipole scattering spectra are negligible, shown in Fig. 4(a). Note that the MD resonant peak is fixed at 590 nm which is the wavelength of the MD transition of Eu^{3+} ($^5D_0 - {}^7F_1$). The result well agrees with the conclusion of the previous work [4]. In fact, as the silver trimer is highly symmetrical for the MD emitters, only MD modes can be excited so that the spontaneous emission behaviors of the MD emitters cannot be effectively tailored in this case. To reduce the symmetry, two silver disks are added near every cell of the silver trimer, forming a silver nonamer [see the inset of Fig. 4(b)]. Surprisingly, the normalized radiative power of the silver nonamer exhibits a dip at the wavelength 590 nm when the MD emitter is put in the center of the silver nonamer, shown in Fig. 4(b).

The suppression of MD scattering power at 590 nm is based on the magnetic anapole state. To validate it, we calculate the Cartesian MD and MTD scattering power of the silver trimer and nonamer, respectively. The Cartesian MD scattering power and MTD scattering power are expressed as

$$P_{\mathrm{sca}}^{\mathrm{MD}} = \frac{c^2k^4Z}{12\pi}|\boldsymbol{m}|^2, \tag{7}$$

$$P_{\mathrm{sca}}^{\mathrm{MTD}} = \frac{c^2k^6Z}{12\pi}|\boldsymbol{T}(m)|^2, \tag{8}$$

where $\boldsymbol{m} = \int \mathrm{d}r^3[\boldsymbol{r}\times\boldsymbol{J}_{\mathrm{sca}}(\boldsymbol{r})]/2c$, $\boldsymbol{T}(m) = -k^2\int \mathrm{d}r^3[r^2\boldsymbol{r}\times\boldsymbol{J}_{\mathrm{sca}}(\boldsymbol{r})]/20$ are Cartesian MD and MTD moments, respectively. The out-of-phase Cartesian magnetic and magnetic toroidal moments cancel each other where $\boldsymbol{m} = -ik\boldsymbol{T}(m)$. Due to the high symmetry of the silver trimer, the Cartesian MTD moment cannot be effectively excited, shown in Fig. 5(a). Besides, the induced circulating near-field distribution shown in Fig. 5(a) indicates a strong MD resonance. As a point source, the amplitude and phase of the MD emitter depending on the spatial distance are divergent. Thus, the asymmetric resonance can be realized even in the rotating symmetric nanostructures. Due to the different separations between the nanodisks and the MD emitter, the remarkable Cartesian MTD moment can be generated in the silver nonamer, shown in Fig. 5(b). The asymmetric distributions of the electric near-field of the three trimers indicated by the gray dashed lines in Fig. 5(b) are the same as the near-field that can excite the onefold ETD moments shown in Figs. 3(b) and 3(c). According to the distribution of the three trimers, the head-to-tail Cartesian ETD moments are generated, leading to the excitation of the Cartesian MTD moment. This physical mechanism is illuminated in Fig. 1(b). Note that the intensity of the electric near-field between the gaps of the three trimers indicated by the gray dashed lines shown in the inset of Fig. 5(b) is very weak, which suggests that the head-to-tail Cartesian ETD moments are excited by the circulating magnetic fields that are associated with asymmetric electric near-field loops of the three trimers. Besides, the trivial magnetic quadrupole scattering power also supports the above analyses. Due to the Cartesian MTD moment formed by the onefold Cartesian ETD moment, it can be excited by the efficient interactions between the MD emitters and the silver nonamer. The suppression of MD scattering of the magnetic anapole state may lead to the suppression of the radiative power of the MD emitter [see Fig. 5(b)].

In addition, the normalized radiative power of the nanosystem is calculated to evaluate the effects of the magnetic anapole state. The normalized radiative power exhibits Lorentzian line shape and is extremely enhanced when the MD emitter is put in the center of the silver trimer, shown in Fig. 6(a). However, based on the magnetic anapole state, the radiative power of the

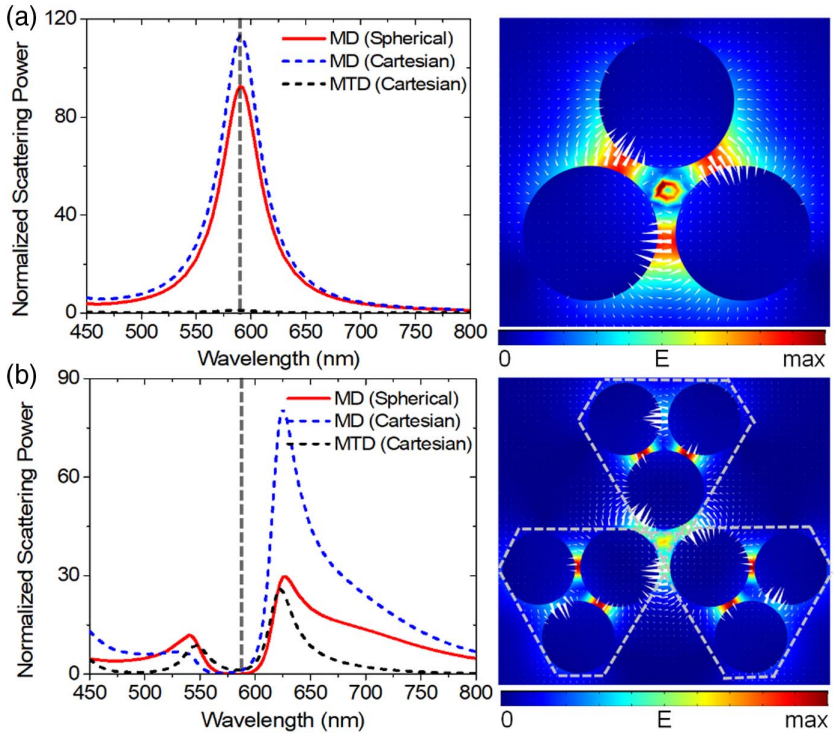

Fig. 5. Contributions of the normalized spherical MD and Cartesian MD and MTD to the radiative powers with the corresponding electric near-field distributions through the center of the silver nanodisks (a) at 590 nm for the trimer and (b) at 590 nm for the nonamer.

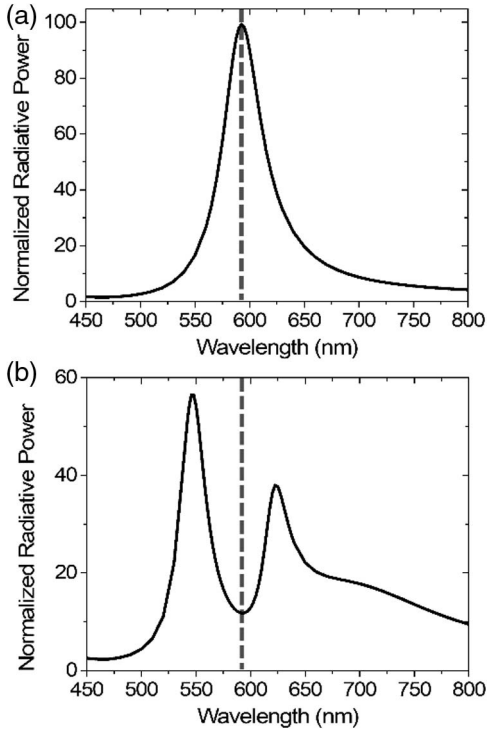

Fig. 6. Radiative power transferred into the far field from an MD emitter placed in the center of the (a) silver trimer and (b) nonamer, respectively.

silver nonamer is remarkably suppressed at the wavelength of 590 nm, shown in Fig. 6(b). Notably, the suppression of the radiative power is mainly based on the interference between the induced modes that are excited by the significant coupling between the emitter and the nanostructure. Different from the previous study, the two strong peaks of the radiative power indicate that the radiative behavior can be tailored in the context that the MD emitter is significantly coupled to the silver nonamer [4]. The suppression of MD radiative power can reduce the radiative loss and can have great implications for the efficient energy transfer.

4. CONCLUSION

In summary, we have demonstrated that MD spontaneous emission behavior can be effectively tailored by the interactions between the emitters and the plasmonic metamolecules. By reducing the symmetry of the nanosystem, the magnetic anapole state associated with the onefold ETD can be excited by the efficient interactions between the MD emitter and the silver oligomers. The magnetic anapole states accompanied by strong suppression of MD scattering can lead to the pronounced suppression of the spontaneous radiative power with the significant coupling between the emitter and the silver nonamer. The efficient enhancement and suppression of MD emission indicate that the spontaneous emission behavior of the MD emitter can be effectively tailored in the context that the MD emitter is significantly coupled to the silver nonamer. These findings not only introduce magnetic anapoles to plasmonics but also set

the foundation for the development of new high-performance magnetic-dipole-based optoelectronic devices.

Funding. Natural Science Foundation of Zhejiang Province (LQ21A040012); Natural Science Foundation of Hunan Province (2021JJ20076); National Natural Science Foundation of China (11704416, 12004362); Changzhou Basic Research Program (CJ20199009).

Disclosures. The authors declare no conflicts of interest.

Data Availability. Data underlying the results presented in this paper are not publicly available at this time but may be obtained from the authors upon reasonable request.

REFERENCES

1. S. Karaveli, S. Wang, G. Xiao, and R. Zia, "Time-resolved energy-momentum spectroscopy of electric and magnetic dipole transitions in Cr^{3+}:MgO," ACS Nano **7**, 7165–7172 (2013).
2. M. Kasperczyk, S. Person, D. Ananias, L. D. Carlos, and L. Novotny, "Excitation of magnetic dipole transitions at optical frequencies," Phys. Rev. Lett. **114**, 163903 (2015).
3. J. Li, N. Verellen, and P. V. Dorpe, "Enhancing magnetic dipole emission by a nano-doughnut-shaped silicon disk," ACS Photon. **4**, 1893–1898 (2017).
4. S. M. Hein and H. Giessen, "Tailoring magnetic dipole emission with plasmonic split-ring resonators," Phys. Rev. Lett. **111**, 026803 (2013).
5. M. Pelton, "Modified spontaneous emission in nanophotonic structures," Nat. Photonics **9**, 427–435 (2015).
6. T. Feng, W. Zhang, Z. Liang, Y. Xu, and A. E. Miroshnichenko, "Isotropic magnetic Purcell effect," ACS Photon. **5**, 678–683 (2018).
7. E. Zanganeh, M. Song, A. C. Valero, A. S. Shalin, E. Nenasheva, A. Miroshnichenko, A. Evlyukhin, and P. Kapitanova, "Nonradiating sources for efficient wireless power transfer," Nanophotonics **10**, 4399–4408 (2021).
8. E. M. Purcell, H. C. Torrey, and R. V. Pound, "Resonance absorption by nuclear magnetic moment in a solid," Phys. Rev. **69**, 37–38 (1946).
9. M. Burresi, T. Kampfrath, D. van Oosten, J. C. Prangsma, B. S. Song, S. Noda, and L. Kuipers, "Magnetic light-matter interactions in a photonic crystal nanocavity," Phys. Rev. Lett. **105**, 123901 (2010).
10. S. Vignolini, F. Intonti, F. Riboli, L. Balet, L. H. Li, M. Francardi, A. Gerardino, A. Fiore, D. S. Wiersma, and M. Gurioli, "Magnetic imaging in photonic crystal microcavities," Phys. Rev. Lett. **105**, 123902 (2010).
11. R. Regmi, J. Berthelot, P. M. Winkler, M. Mivelle, J. Proust, F. Bedu, I. Ozerov, T. Begou, J. Lumeau, H. Rigneault, M. F. Garcá-Parajó, S. Bidault, J. Wenger, and N. Bonod, "All-dielectric silicon nanogap antennas to enhance the fluorescence of single molecules," Nano Lett. **16**, 5143–5151 (2016).
12. M. Sanz-Paz, C. Ernandes, J. U. Esparza, G. W. Burr, N. F. van Hulst, A. Maitre, L. Aigouy, T. Gacoin, N. Bonod, M. F. Garcia-Parajo, S. Bidault, and M. Mivelle, "Enhancing magnetic light emission with all-dielectric optical nanoantennas," Nano Lett. **18**, 3481–3487 (2018).
13. E. Zanganeh, A. Evlyukhin, A. Miroshnichenko, M. Song, E. Nenasheva, and P. Kapitanova, "Anapole meta-atoms: nonradiating electric and magnetic sources," Phys. Rev. Lett. **127**, 096804 (2021).
14. A. E. Miroshnichenko, A. B. Evlyukhin, Y. F. Yu, R. M. Bakker, A. Chipouline, A. I. Kuznetsov, B. Luk'yanchuk, B. N. Chichkov, and Y. S. Kivshar, "Nonradiating anapole modes in dielectric nanoparticles," Nat. Commun. **8**, 8069 (2015).
15. T. Feng, Y. Xu, W. Zhang, and A. E. Miroshnichenko, "Ideal magnetic dipole scattering," Phys. Rev. Lett. **118**, 173901 (2017).
16. K. V. Baryshnikova, D. A. Smirnova, B. S. Lukyanchuk, and Y. Kivshar, "Optical anapoles: concepts and applications," Adv. Opt. Mater. **7**, 1801350 (2019).
17. V. Savinov, N. Papasimakis, D. P. Tsai, and N. I. Zheludev, "Optical anapoles," Commun. Phys. **2**, 69 (2019).
18. G.-M. Pan, F.-Z. Shu, L. Wang, L. Shi, and A. B. Evlyukhin, "Plasmonic anapole states of active metamolecules," Photon. Res. **9**, 822–828 (2021).
19. E. Díaz-Escobar, T. Bauer, E. Pinilla-Cienfuegos, Á. I. Barreda, A. Griol, L. Kuipers, and A. Martínez, "Radiationless anapole states in on-chip photonics," Light Sci. Appl. **10**, 204 (2021).
20. A. G. Lamprianidis and A. E. Miroshnichenko, "Excitation of nonradiating magnetic anapole states with azimuthally polarized vector beams," Beilstein J. Nanotechnol. **9**, 1478–1490 (2018).
21. E. A. Gurvitz, K. S. Ladutenko, P. A. Dergachev, A. B. Evlyukhin, A. E. Miroshnichenko, and A. S. Shalin, "The high-order toroidal moments and anapole states in all-dielectric photonics," Laser Photon. Rev. **13**, 1800266 (2019).
22. Z.-J. Yang, Y.-H. Deng, Y. Yu, and J. He, "Magnetic toroidal dipole response in individual all-dielectric nanodisk clusters," Nanoscale **12**, 10639–10646 (2020).
23. P. Kapitanova, E. Zanganeh, N. Pavlov, M. Song, P. Belov, A. Evlyukhin, and A. Miroshnichenko, "Seeing the unseen: experimental observation of magnetic anapole state inside a high-index dielectric particle," Ann. Phys. **532**, 2000293 (2020).
24. V. A. Fedotov, A. V. Rogacheva, V. Savinov, D. P. Tsai, and N. I. Zheludev, "Resonant transparency and non-trivial non-radiating excitations in toroidal metamaterials," Sci. Rep. **3**, 2967 (2013).
25. Y. Yang and S. I. Bozhevolnyi, "Nonradiating anapole states in nanophotonics: from fundamentals to applications," Nanotechnology **30**, 204001 (2019).
26. Y. Lu, Y. Xu, X. Ouyang, M. Xian, Y. Cao, K. Chen, and X. Li, "Cylindrical vector beams reveal radiationless anapole condition in a resonant state," Opto-Electron. Adv. **5**, 210014 (2022).
27. P. Nordlander and C. Oubre, "Plasmon hybridization in nanoparticle," Nano Lett. **4**, 899–903 (2004).
28. M. Celebrano, X. Wu, M. Baselli, S. Großmann, P. Biagioni, A. Locatelli, C. De Angelis, G. Cerullo, R. Osellame, B. Hecht, L. Duò, F. Ciccacci, and M. Finazzi, "Mode matching in multiresonant plasmonic nanoantennas for enhanced second harmonic generation," Nat. Nanotechnol. **10**, 412–417 (2015).
29. G.-M. Pan, D.-J. Yang, L. Zhou, Z.-H. Hao, and Q.-Q. Wang, "Enhanced second harmonic generation by mode matching in gain-assisted double-plasmonic resonance nanostructure," Sci. Rep. **7**, 9776 (2017).
30. D. Dregely, M. Hentschel, and H. Giessen, "Excitation and tuning of higher-order Fano resonances in plasmonic oligomer clusters," Nano Lett. **5**, 8202–8211 (2011).
31. N. Liu, S. Mukherjee, K. Bao, Y. Li, L. V. Brown, P. Nordlander, and N. J. Halas, "Manipulating magnetic plasmon propagation in metallic nanocluster networks," Nano Lett. **6**, 5482–5488 (2012).
32. R. Verre, Z. J. Yang, T. Shegai, and M. Kall, "Optical magnetism and plasmonic Fano resonances in metal–insulator–metal oligomers," Nano Lett. **15**, 1952–1958 (2015).
33. E.-M. Roller, L. K. Khorashad, M. Fedoruk, R. Schreiber, A. O. Govorov, and T. Liedl, "DNA-assembled nanoparticle rings exhibit electric and magnetic resonances at visible frequencies," Nano Lett. **15**, 1368–1373 (2015).
34. B. Ögüt, N. Talebi, R. Vogelgesang, W. Sigle, and P. A. Van Aken, "Toroidal plasmonic eigenmodes in oligomer nanocavities for the visible," Nano Lett. **12**, 5239–5244 (2012).
35. Y. Bao, Z. Hu, Z. Li, X. Zhu, and Z. Fang, "Magnetic plasmonic Fano resonance at optical frequency," Small **11**, 2177–2181 (2015).
36. G.-M. Pan, D.-J. Yang, L. Zhou, and Z.-H. Hao, "Low-loss resonance modes in a gain-assisted plasmonic multimer," J. Phys. D **51**, 115104 (2018).
37. Z. Qian, Z. Li, H. Hao, L. Shan, Q. Zhang, J. Dong, Q. Gong, and Y. Gu, "Absorption reduction of large Purcell enhancement enabled by topological state-led mode coupling," Phys. Rev. Lett. **126**, 023901 (2021).

38. H. Wei, X. Yan, Y. Niu, Q. Li, Z. Jia, and H. Xu, "Plasmon-exciton interactions: spontaneous emission and strong coupling," Adv. Funct. Mater. **31**, 2100889 (2021).
39. A. C. Valero, E. A. Gurvitz, F. A. Benimetskiy, D. A. Pidgayko, A. Samusev, A. B. Evlyukhin, V. Bobrovs, D. Redka, M. I. Tribelsky, M. Rahmani, K. Z. Kamali, A. A. Pavlov, A. E. Miroshnichenko, and A. S. Shalin, "Theory, observation, and ultrafast response of the hybrid anapole regime in light scattering," Laser Photon. Rev. **15**, 2100114 (2021).
40. H. Kim, S. Z. Uddin, N. Higashitarumizu, E. Rabani, and A. Javey, "Inhibited nonradiative decay at all exciton densities in monolayer semiconductors," Science **373**, 448–452 (2021).
41. L. Cumming, "Ampere's rule," Nature **34**, 192–193 (1886).
42. D. J. Jackson, *Classical Electrodynamics*, 3rd ed. (Wiley, 1998).
43. A. Nazir, S. Panaro, R. Proietti Zaccaria, C. Liberale, F. De Angelis, and A. Toma, "Fano coil-type resonance for magnetic hot-spot generation," Nano Lett. **14**, 3166–3171 (2014).
44. D.-J. Yang, S.-J. Im, G.-M. Pan, S.-J. Ding, Z.-J. Yang, Z.-H. Hao, L. Zhou, and Q.-Q. Wang, "Magnetic Fano resonance-induced second-harmonic generation enhancement in plasmonic metamolecule rings," Nanoscale **9**, 6068–6075 (2017).
45. S.-D. Liu, P. Yue, S. Zhang, M. Wang, H. Dai, Y. Chen, Z.-Q. Nie, Y. Cui, J.-B. Han, and H. Duan, "Metasurfaces composed of plasmonic molecules: hybridization between parallel and orthogonal surface lattice resonances," Adv. Opt. Mater. **8**, 1901109 (2020).
46. P. B. Johnson and R. W. Christy, "Optical constants of the noble metals," Phys. Rev. B **6**, 4370–4379 (1972).
47. P. Grahn, A. Shevchenko, and M. Kaivola, "Electromagnetic multipole theory for optical nanomaterials," New J. Phys. **14**, 093033 (2012).
48. D. Sikdar, W. Cheng, and M. Premaratne, "Optically resonant magneto-electric cubic nanoantennas for ultra-directional light scattering," J. Appl. Phys. **117**, 083101 (2015).